Original Article

An EMG-driven biomechanical model of the canine cervical spine

M. Alizadeh [a]*, G.G. Knapik [a], J.S. Dufour[a] , C. Zindl[b], M.J. Allen[b,c], J. Bertran[c], N. Fitzpatrick[d], W.S. Marras[a]

[a] *Spine Research Institute, The Ohio State University,* 520 *Baker Systems, 1971 Neil Avenue., Columbus OH 43210 USA*

[b] *Surgical Discovery Center, Department of Veterinary Medicine, University of Cambridge, Madingley Road, Cambridge, CB3 0ES, UK*

[c] *Department of Veterinary Clinical Sciences, The Ohio State University, Columbus, Ohio 43210 USA*

[d] *Fitzpatrick Referrals, Eashing, Surrey GU7 2QQ, UK*

* Corresponding author.

E-mail address*:* Alizadeh.3@osu.edu (Name: Mina Alizadeh).

Postal address: The Ohio State University, Spine Research Institute, 1971 Neil Avenue, Room 520, Columbus, OH 43210

Abstract

Background: In spite of the frequency of cervical spine injuries in canines, a biomechanical understanding that enables one to investigate the risk of neck disorders associated with physical activities and external loads, and surgical procedures has not been developed. The purpose of this effort was to develop an EMG-driven dynamic model of the canine cervical spine to assess the load profile imposed upon the canine neck during physical exertions.

Methods: a canine subject was recruited in this investigation in order to collect subject specific data. Reflective markers and motion capture system were used for kinematic measurement; surface electrodes were used to record electromyography signals, and with the aid of force plate kinetics were recorded. 3-D model of the canine subject were reconstructed from MRI dataset. Muscles lines of action were defined through a new technique with the aid of 3D white light scanner.

Results: The reliability of the model was investigated by comparing the resultant dynamic measured external moment to the predicted internal moment in both the sagittal and axial planes via correlation coefficient (R^2) and average absolute error (AAE). The model performed well with a 0.73 weighted R^2 value in all three planes. The weighted average absolute error of the predicted moment was less than 10% of the external moment.

Interpretation: The proposed model is a canine specific forward-dynamics model that precisely tracks the canine subject head and neck motion, calculates the muscle force generated from the twelve major moment producing muscles, and estimates resulting loads on specific spinal tissues.

Keywords: dog; neck; electromyography, dynamic, kinematics.

1. Introduction

The canine's cervical spine is particularly susceptible to trauma because of the large moment generated by the head relative to the base of the spine (Breit and Künzel, 2004; Crisco et al., 1990; Jeffery et al., 2013). In order to develop a better understanding of preventive strategies and effective therapeutic interventions, a more quantitative appreciation of canine cervical spine biomechanics is desirable, since a detailed biomechanical knowledge of the frequent sites of cervical spine injury is required. Biologically-assisted biomechanical models provide a viable environment to understand spine tissue loading in vivo. Once developed, these models are capable of helping to understand potential injury risk by accounting for how muscles are dynamically recruited and how the patterns of muscles recruitments collectively impose forces on tissues under various daily activities. It is believed this model will significantly help to understand canine cervical spine kinematics which is still not well understood (Johnson et al., 2011). In addition, such model can help us understand the implications of contemplated surgeries on the biomechanical behavior of the spine. Beyond the application of canine cervical spine biomechanical models in veterinary medicine, these models could be used further to better understand complex biomechanical relationships and the knowledge gained can be translated and applied to human spine models. In vivo studies on canines can be easily conducted and used to validate overall subject-specific model outputs. Moreover, this model will provide a suitable platform to explore the validity of canine cervical spine models that have been employed extensively for investigating effects of spinal instruments developed for human spine (Autefage et al., 2012; Lim et al., 1994; Sharir et al., 2006; Sheng et al., 2010). Several human cervical spine models have been developed and validated to better understand the mechanical loads on the human spine (Horst et al., 1997; Hyeonki Choi, 2010; Jager et al., 1996; Lopik and Acar,

2007; Snijders et al., 1991; Stemper et al., 2004; Vasavada et al., 1998). In spite of the high frequency of spinal injuries observed in canines (Foss et al., 2013; Jeffery et al., 2013), attempts to develop models for the canine cervical spine have been lacking, to our knowledge.

Since the muscles surrounding the spine are the major contributors to spine loading, a critical component of a biomechanical model is the ability for the model to accurately estimate muscle force. Since the cervical spine and its muscles are a statistically indeterminate system, cervical spine biomechanical models utilize one of two approaches to compute muscle forces: inverse dynamics or biologically-assisted (electromyography or EMG-driven) techniques, (Choi and Vanderby Jr, 1999; Cholewicki and McGill, 1994). In spite of the popularity of inverse dynamic driven models, they have fairly significant shortcomings. Inverse dynamics models are appropriate in highly dynamic (impulse) loading situations such as whiplash, where muscles do not have enough time to activate and alter tissue loading (Huber, 2013) and for static exertions. However, during activities of daily living, which represent the vast majority of lifetime exposures, inverse dynamics models cannot account for the complex co-contraction of antagonist muscles surrounding the spine. Studies have shown that significant muscle coactivations occur in the muscles surrounding the lumbar spine in humans and that accounting for these coactivities profoundly increases spinal load predictions compared to inverse dynamic models that assume no coactivity (Granata and Marras, 1995). It has been suggested that muscle forces, on average, can be as high as 218% greater in lateral bending and 123% greater in flexion/extension in EMG-driven models of the lumbar spine compared to inverse dynamic models (Cholewicki et al., 1995). It is expected that these underestimations would be even greater in the cervical spine since the relatively small mass of the head may require larger amounts of coactivity to protect it from perturbations and keep it in a stable state. We expect that inverse dynamics models would

92 severely underestimate cervical spine tissue loading (Hyeonki Choi, 2010). Hence, the EMG-
93 driven biomechanical modeling approach would be expected to enable a much better estimation
94 of spinal loads since it accounts for realistic antagonist muscle cocontraction during dynamic
95 physical activities. In addition, EMG-driven models also account for the individual variability
96 across subjects and conditions in muscle recruitment.

97 Therefore, the objective of this study was to develop a canine specific EMG-driven
98 cervical spine model that would be sensitive to dynamic physical exertions of the cervical spine
99 and capable of accurately predicting internal moments and spinal tissue loading profiles.

100

101 **2. Methods**

102 2.1 Modeling approach

103 We applied well developed human spine modeling concepts to to the development of a
104 canine cervical spine biomechanical model (Marras and Granata, 1997; Theado et al., 2007). In
105 order to build the EMG-driven model, several experimentally measured parameters including
106 kinematic information, kinetic profiles, muscles of canine cervical spine structure, and EMG
107 signals were incorporated as model inputs to predict the resultant internal moments and spinal
108 loads as model outputs (Fig.1). The underlying logic of the model assumes that the key to precise
109 estimation of spinal loads is to understand how the internal tissues respond to physical exertions
110 and activities and estimate tissues force contributions to the system. Below we briefly describe
111 how the model inputs were acquired and implemented into the model.

112 2.1.1 Muscle modeling

Muscle function is represented as a three-dimensional vector function of force magnitude and force direction via dynamic muscle lines of action. Dynamic tensile force of a muscle (j) is estimated (eq.1) as the product of muscle gain ratio ($GainRatio_j$), EMG (EMG_j), muscle cross-section area ($Area_j$), while taking into account the force-length ($f(L_j(t))$) and force-velocity ($f(V_j(t))$) relationship of the muscles (Theado et al., 2007). Moment generated by the muscles (M) were calculated via summation of vector products between muscle (j) tensile force (F) and its moment arm (r) at every time point during the dynamic trial (eq.2) (Theado et al., 2007).

Muscle moment arm is defined as the perpendicular distance of muscle line of action from the joint axis of rotation (Vasavada et al., 1998). The model is operating such that the gain ratio for each muscle was predicted within a calibration trial, in order to personalize muscle forces for the canine subject similar to the technique that was developed by Dufour et al. (2013) for human lumbar spine muscles. A simple flexion/extension trial was selected as a calibration trial. Once these parameters for each muscle were specified, they were applied to analyze other trials performed by the canine subject such as lateral bending and axial rotation tasks. In order to accurately estimate muscle gain ratio, an optimization algorithm had been used to minimize error between muscles' internal moments and external moments about cervical spine joints. Internal moments included those generated by muscles and ligaments while external moments included those imposed by external force measured from the force plate and the inertial contributions of the head and vertebral bodies. Based on the anatomical properties of muscles in this model, the objective function of calibration algorithm aimed to minimize moment prediction errors in two joints, C1/C2 and C7/T1. The boundary conditions for the calibration procedure used here were originally developed for the human lumbar spine. However, previous studies have shown

relatively similar muscle parameters between humans and canines (McCully and Faulkner, 1983). Therefore, these parameters should serve as a good starting point until boundaries for normal canines can be developed.

$$F_j(t) = GainRatio_j . Area_j . EMG_j(t) . f\left[L_j(t)\right] . f\left[V_j(t)\right] \quad (1)$$

$$\vec{M} = \sum_{j=1}^{10} \vec{r_j}(t) \times \vec{F_j}(t) \quad (2)$$

Since there is currently a lack of comprehensive canine neck muscle properties to approximate muscle lines of action and cross-sectional areas, the best technique for determining these parameters for this model had to be determined. Medical imaging techniques and cadaveric experiments are two of the most well established methods to measure muscle moment arms and to define muscle line of action (Dumas et al., 1991; Macintosh and Bogduk, 1991; Németh and Ohlsén, 1986). However there are many sources of inaccuracies associated with these techniques. First, and the most probable shortcoming was that of the partial volume effect phenomena, where a large bias can be introduced in measured parameters on medical images (Soret et al., 2007). Second, scan planes are generally perpendicular to the scan table while the direction of the muscles are most probably oblique to the scan plane, consequently CSA derived from images are typically overestimated (Jorgensen et al., 2003). Adjusting the CSA for muscle fiber angle can reduce this error, however, muscle fiber directions are often not detectable via MRI. Considering individual variability across subjects, it is impossible to correct CSA for the subject-specific models with medical images. Third, distinguishing muscles and separating them from one another requires a thorough knowledge of cross-sectional anatomy as well as powerful MRI imaging to be able to visually differentiate muscles. In order to reduce error introduced by

these limitations in the model, an alternative approach was investigated to determine muscle line of action.

The application of a three-dimensional white light scanner (3DWLS) (Artec Eva, Artec, Palo Alto, CA, USA) to determine muscle lines of action while minimizing medical imaging shortcomings was investigated. The Artec Eva 3D scanner consists of a portable camera that dynamically captures 3D geometry data and surface information at up to 15Hz. It is an ideal tool for medical scanning purposes because: a) the 3D scanner is able to provide a 3D view of an object to help identify cervical spine muscles in their complex geometrical arrangement; and, b) the scanner is capable of providing high resolution images while capturing texture at high speed. One advantage of this approach is that measurements such as fiber angles and muscle cross-sections are taken directly from intact muscles without disturbing muscle attachments. Therefore, more accurate measurements in comparison to previous direct dissection cadaveric studies would be expected. A cadaver dog, euthanized for another research protocol unrelated to this study was used to test the proposed technique for determining canine cervical muscle lines of action. The cadaver dog was relatively similar to the canine subject we recruited for model development in many aspects such as breed, weight and size.

The dog specimen dissection process started by removing the skin and underlying fatty layers until most of the superficial muscle was exposed. Then, the 3D scanner was used to scan the exposed muscle. Next, every single muscle in the neck region was removed carefully one at a time, and the 3DWLS was used to capture the surface information of the next layer of exposed intact muscle. The 3DWLS data was then post processed to evaluate the variability of the fiber directions throughout the length of each muscle. Muscle volume was then defined as a volume between two consecutive scans obtained in the order as described previously. Each muscle's line

of action was then approximated by the three dimensional centroid path of that muscle (Jaeger et al., 2011). The muscle centroid line was achieved by connecting the central points of the muscle cross-section in transverse planes. Those planes were defined as surfaces parallel to the vertebral bodies' endplates with small distance as much as 5 mm from each in order to increase the accuracy (Jaeger et al., 2011). Finally, to reduce modeling complexity for this first stage, a straight line was fitted to the centroid path obtained by multiple planes and further used as the straight muscle line of action.

Among the many muscles in the neck, six pairs representing the power producing muscles were selected for modeling purposes. Muscles were chosen based on their moment arm length, their cross-sectional area, and their accessibility via surface electromyography electrodes. These twelve muscles (six muscle pairs), left/right sternomastoid, left/right obliquus capitis, left/right splenius, left/right biventer, left/right complexus, and left/right longissimus lines of action are shown in Figure 6. As mentioned earlier, we had recorded EMG signals for only four pairs of muscles while there are six pairs of muscles in the model. Anatomically, splenius is located dorsal to the biventer and complexus, with larger cross-sectional area and moment arm compared to muscles underneath such as the biventer and complexus. This indicated that more activation expected to be seen from splenius than biventer and complexus. Considering the capability of surface electrodes on detecting different signals, it was not practical to locate separate electrodes for splenius, biventer and complexus. Therefore, we recorded splenius activity by EMG electrodes and we assumed the same recruitment pattern shape would apply to biventer and complexus.

2.1.2 Geometry reconstruction

In order to generate the subject-specific anatomical model, the canine subject underwent MRI imaging. A series of image processing operations were then performed on the MRI images in order to obtain a detailed three-dimensional model of the canine cervical spine (Skull - T1). The head and neck posture then were realigned to match the neutral standing posture.

2.1.3 Ligaments and intervertebral disc modeling

Ligaments were modeled as passive force vectors located between two points representing ligament attachment points. Ligament attachments in the model were adopted based on anatomy literature (Kumar, 2012). The nuchal ligament, dorsal atlanto-occipital membrane, lateral atlanto-occipital membrane, dorsal atlanto-axial ligament, ventral atlanto-axial membrane, alar ligament, transverse atlantal ligament, apical ligament, alar ligament, apical ligament, ventral longitudinal ligament, dorsal longitudinal ligament, yellow ligament, interspinous ligament, and capsular ligament were all incorporated in the model. The width of the ligament was represented using multi force vectors to ensure that the force could encompass all the physiological width of the ligament. Due to the lack of canine ligament properties, human cervical spine ligament properties were used in the model instead (Han et al., 2012). Intervertebral disc geometry at each level was reconstructed from the MRI dataset and its material properties obtained from the literature (Zimmerman et al., 1992). They were modeled as three dimensional spring dampers located at the center of the disc space for each motion segment. Therefore, at each spinal joint there is an intervertebral disc and anatomically match ligaments in order to stabilize the joint. The atlanto-occipital and atlanto-axial are two complex joint with a shared common joint capsule. Due to modeling limitations, assumptions were taken

to construct these joints. Cartilage at these joints was modeled as three dimensional spring dampers with stiffness properties similar to cartilage stiffness (Jaumard et al., 2011). In addition, with a defined contact forces at these joints the vertebral bodies distance were preserved without increasing spinal load drastically. The final 3D dynamic model of canine cervical spine is shown in Figure.2.

2.2 Modeling approach

2.2.1 Experimental tasks and training

A skeletally mature male hound (26.0 kg body weight) served as a subject in this investigation. The dog was examined by a veterinarian and documented to be healthy, with no evidence of joint or spinal disease. The dog was housed in a room with other dogs and was fed a standard laboratory dog chow with water *ad libitum*. During the three weeks before the data collection, the dog was trained using food treats to allow for passive manipulation of the head and neck via a soft head collar (Gentle Leader, Suffolk, UK). Beginning from the neutral position, the head and neck were slowly moved through a range of motion from full extension (nose pointing up towards the ceiling) to full flexion (nose down towards the floor). Movements were then repeated for side to side motions and for oblique motions. After going through all motion sequences, a latex resistance band (TheraBand, Akron, OH, USA) was attached to the head collar around the mandibular region and the end of the resistance band was manually fixed on the floor, so that no traction was applied with the head in neutral position. The sequence of passive head/neck movements was then repeated with the resistance band in place. In order to slowly acclimate the dog to the resistance, training during the first week was

carried out with a band of medium resistance and during subsequent training sessions (week 2 and 3) and at the testing day with a band of significantly higher resistance.

2.2.2 Subject

One trained dog was enrolled in this experiment to perform several exertion trials in a room equipped with a motion capture system and force plate. The experimental procedures for this study were reviewed and approved by the local institutional animal care and use committee (IACUC). The dog was acclimated to the experiment space 15-20 minutes before subject preparation. In order to activate muscles, the dog was required to pull against a latex band attached between its collar and the force plate during various exertion trials ranging from simple flexion/extension to more complex exertions including axial rotation and lateral bending similar to the training movements (Fig.3). During the experiment, the dog was encouraged to follow food treats in the hand of the trainer to resemble the training procedure.

2.2.3 Data collection system (Apparatus)

Bipolar surface electrodes were placed over 8 neck muscles (four pairs of muscles). EMG data was collected with a MA300-XVI Advanced Multi-channel EMG System (Motion Lab Systems Incorporated, Baton Rouge, Louisiana,USA) at 1000 HZ collection frequency. The latex resistance band force and moment were measured via a force plate (Bertec 4060A; Bertec, Worthington, OH, USA). An OptiTrack optical motion capture system (NaturalPoint, Corvallis, OR, USA) with 24 Flex 3 infrared cameras was used to capture optical marker locations during the experiment via OptiTrack's Motive software. Custom software developed at the Ohio State University Spine Research Institute was used to record analog signals through a NI USB-6225

Data Acquisition Device (National Instruments, Austin, TX, USA) and to control and sync optical data collection.

2.2.4 Kinematic and kinetic data acquisition

Three reflective markers (optical) were attached to the bony landmarks of head: 1) left frontal process, 2) right temporozygomatic bone, and 3) left nasal bone. Three more markers were attached to a small solid panel made of plastic that was tightly secured to the back of the dog to serve as a rigid body. Three more reflective markers were glued to the neck approximately on the spinous process of C2, C5 and C7 and two more on the head of the scapula to represent shoulder movement (Fig.4). The optical marker locations were recorded during each trial by the motion capture system. Optical marker position data were then used to calculate the kinematics of the head, neck and back referenced to the ground in a neutral posture which was recorded prior to experimental tasks. Developing a multi-segmental model allowed us to define angular displacement for each joint based on the data recorded by the motion capture system.

Force and moment data from the force plate were used to measure dynamic external force exposures during each trial. Inertial moment contributions of the head and vertebral bodies were added to the force plate measured moments and served to define the total external moment.

2.2.4.1 Muscle EMG Data Acquisition

EMG activities of the four pairs of extensor/flexor neck muscles were recoded using surface electrodes. These muscles consisted of: left/right obliquus capitis, left/right splenius, left/right longissimus, and left/right sternocleidomastoid (Fig.5). These muscles were chosen since they are all major power producing neck muscles based on their cross-section area, and functionality.

The EMG electrodes were located on the shaved skin based upon a study of the anatomical description of muscle locations (Alizadeh et al, 2016). The skin preparation was similar to previously published paper (Marras and Davis, 2001).

An MRI imaging session was scheduled after the experimental session in order to precisely document the anatomical features of the vertebral bodies. T1 and T2 weighted MRI images were acquired on a 3T MRI scanner (Magnetom Trio, Siemens Healthcare, Erlangen, Germany). Transverse slices of 1 mm thickness were obtained from the skull level and extended caudally to the level of the second thoracic vertebra. This imaging session was also used to validate the EMG electrode and optical marker location. The locations of the EMG electrodes were indicated with diagnostic MRI markers. These markers showed up well in the imaging allowing each electrode to be paired with the correct target muscle. In addition, custom made dual modality markers were used to line up optical motion capture data with the MRI data. These consisted of diagnostic MRI markers embedded within optical motion capture markers (Fig.6).

3 Results

3.1 Validation

Based on the findings of Dufour et al. (2013), the acceptable range for gain ratio of 6-131 N/cm^2V was adopted to represent the physiological acceptable range of gain in humans (Granata and Marras, 1993). The gain ratio for each muscle calculated in this study was between 30-80, which fell within the predicted physiological range previously reported for human spine.

The reliability of the model was investigated by comparing the resultant dynamic measured external (to the body) moment to the predicted internal moment produced by the muscles and ligaments in both the sagittal and axial planes via their correlation coefficient (R^2) and average

absolute error (AAE). Comparison of the measured external moment and the predicted internal moment (over time) is illustrated in Figure 7. Since the moments generated in the lateral planes were negligible compare to sagittal and axial planes, most probably signals are basically noise. Therefore, planar R^2 would not be an appropriate measure for lateral plane. The model performed well with a 0.73 weighted R^2 value in all three planes, considering each plane contribution in generated moment. The weighted average absolute error of the predicted moment was less than 10% of the external moment in the calibration trial.

3.2 Spinal load

Figure 8 shows the peak spinal load at all the levels during the trial. The injury force tolerance threshold for canine cervical spine has not been defined. Therefore, we will only comment on the spine loading pattern in a relative fashion. Compression forces gradually increased from C1/C2 to C5/C6 where they were the greatest then these forces gradually decreased to C7/T1. The anterior/posterior (A/P) and lateral (Lat) forces varied along the length of the cervical spine.

4. Discussion

It must be emphasized that all models, in general, are simplifications of a real situation. However, for the first time, we have been able to develop a dog-specific cervical spine biomechanical model that helps us understand the pattern of 3D moments and forces imposed upon the vertebral tissues of the spine during a complex dynamic exertion made by a live animal. The model developed by the authors was an EMG-driven hybrid model that predicted muscle generated moments and determined spinal loads. EMG signals were used as a measure to document the physiological pattern of muscle recruitment and optimization algorithms were implemented in order to personalize the model by comparing moments about three axes of the

vertebral joints. The proposed model attempted to accurately and realistically represent the mechanical loading and behavior of the neck structure, The EMG-driven canine neck model predicted spinal loads as a result of twelve major canine neck muscle activities as a response to physical exertions and external loads. The model was capable of estimating compression, anterior/posterior, and lateral shear forces of the canine cervical spine at each level from C1-T1. In order to interpret injury risk based on calculated spinal loads, canine specific disc failure threshold values would be needed. Unfortunately, such information is not available in the literature. One might consider adopting human threshold limits as a surrogate. However, the extreme difference between human and canine cervical spine in many aspects such as the range of motion, material properties, and disc size, would suggest that this may not be a reasonable quantitative comparison.

The compression spine loads indicated a reasonable and expected pattern of loading, where the highest compression values occurred at the C4/C5 level, similar to that reported by Yoganandan et al., (2001) in the human cervical spine. It is not advisable to validate model fidelity by quantifying spinal loads magnitude, since there is no experimental data on canine cervical spine failure threshold to our knowledge. Moreover, due to the significant differences between human and canine cervical spine ranging from tissue material properties to postural variation and type of physical activities they are exposed to, it is not reasonable to compare them. A similar argument can be made for the muscle forces and moments. One might consider the magnitude of internal moments and spinal loads observed during the trial (Fig. 8) to be very large. However, when considering the fact that the dog was pulling forcefully against a strong latex resistance band, these spine loading magnitudes are not out of the range of possibilities in the exertions may be close to a maximum exertion for the animal.

The current EMG-driven dynamic model is unique in that it was dog specific in terms of: (1) muscle morphometric properties such as CSA, (2) muscle line of action, (3) muscle activities, and (4) subject kinematics. The model structure is multi-dimensional and is capable of considering dynamic responses of the subject. Neck moments and tissue loads are derived from dynamic muscle force vectors and internal neck muscle moment arms. These parameters were estimated based upon the EMG activity of 12 cervical spine muscles during the physical exertion, while considering muscle moment generation potential which greatly depends on the motion of the different canine body segments and resulting muscle moment arms. The surface EMG signals of the major force producing muscles of the canine neck, along with muscle force-length and force-velocity relationships were employed to estimate muscle forces.

This model represents a significant advancement in understanding the biomechanics of canine cervical spine in several respects. First, this is a multi-segmental cervical spine model in which Skull-T1 motion segments are separated and are allowed to move relative to each other. The advantage of the multi-segmental cervical spine can be emphasized at the atlanto-occipital and atlanto-axial joints. According to (Dugailly et al., 2011), 40% of axial rotation occurs at the atlanto-axial joint, with the rest being distributed along the rest of the neck. This allowed us to define angular displacement for each joint based on the data recorded by the motion capture system. As a result, the error introduced into the model by implementing the calculated joint angles from the recorded data of motion capture system was less than 0.5 mm. Therefore, the model motion was almost identical to the actual dog motion. It is believed that while the joint kinematics are precisely defined in the model, muscle moment arm and consequently measured internal moment at each time point during the trial will be estimated more accurately.

Second, the exertion that was used for calibration and later was modeled represents a complex motion including axial rotation and lateral bending while the dog was fully extending his neck from a deep flexed posture, since constraining the dog to a specific range of motion was impossible based upon the objective of the experiment which was to let the dog activate the neck muscles naturally while performing extreme range of motion exertions. Therefore, it can be claimed that the model is strong enough to respond a complex motion in spite of the model limitations.

Third, a non-MVC calibration technique was used to determine personalized muscle gain ratios. Since it would be impossible to obtain a true MVC in a canine specimen, and even in humans MVCs can be sensitive to fatigue, posture, exertion type and pain on the exertion, the non-MVC calibration technique proved to be very affective. The fidelity and robustness of this technique is well established over a variety of complex exertions for humans (Dufour et al., 2013). As described in the method section, in the presented model upper and lower bounds for gain ratio was set based on the range reported by Dufour et al., (2013). We believe even though this range was obtained for human lumbar spine, it is expected to be valid for this individual canine since determined gain ratios were well within the boundaries. Further studies will need to be performed to determine physiological gain ratio limits for canines.

Fourth, the muscle lines of action were determined in a cadaver-based experiment with a precise technique. The advantages of this technique in comparison to the previously established cadaver experiments were: 1) muscle measurements such as cross sectional area were achieved without disturbing muscle attachments, 2) muscle cross sectional areas could be measured at any level, and 3) estimated muscle lines of action were represented realistically since they were fitted

to the muscle centroid curve created by connecting muscle centroids in various planes, corrected for muscle fibers angle.

As with any assessment tool one must appreciate the limitations of the model. First, it should be noted that this model was developed based on data from a single animal subject. Therefore, the estimated muscle properties including initial muscle length, CSA, line of action are unique to this animal and are not necessarily representative of all canines. Another limitation associated with the performance of the model is that at the beginning of the trial a strong correlation between the predicted and measured moments were not observed. However, one must consider that during the first quarter of the trial, the dog was not pulling against the latex band due to the deep flexed posture of the neck. Thus, measured external moments for this portion of the task were negligible, while internal moments were registered from the muscles. This discrepancy may be due to limitations in the way inertial characteristics were estimated for the head and vertebrae. Better approximations for these unknown variables will need to be determined in the future. In addition, there were several parameters in the model such as gain ratio constraints and ligament material properties that had been taken from a well-established human spine model. Further investigation is necessary to determine more representative parameters for canines. Finally, further exploration should be done in order to model atlanto-occipital and atlanto-axial joints physiologically matched with proper tissue properties for canine cervical spine. In spite of these procedural limitations, we believe this effort represents a significant step forward in quantifying spine loads within the spine of a canine.

5. Conclusions

The model described in this article is the first known EMG-driven model for the canine cervical spine. We believe the presented model is an important achievement in terms of application of engineering principals to veterinary medicine. The developed model represents a significant step toward implementing biomechanical modeling capabilities to understand underlying mechanisms of the canine cervical spine non-invasively, although there are still many unknowns relative to the canine cervical spine including kinematics and kinetics (Johnson et al., 2011). The model met the objectives well by being able to track the motion precisely, accurately predict internal moments of cervical spine based on the measured external moments, and estimate spinal tissue loads that are reasonable based on the task that was performed. It is believed this model represents a significant step toward building advanced canine biomechanical cervical spine models for future investigations. Such an advanced canine specific model could be eventually used by veterinary orthopedic and rehabilitation centers routinely to evaluate treatment strategies and surgical techniques before applying them on the canine patient.

Conflict of interest statement

None declared.

Acknowledgements

This work was supported in part by Fitzpatrick Referrals Ltd., through the One Health/One Medicine Fellowship at The Ohio State University.

References

Alizadeh, M., Zindl, C., Allen, M.J., Knapik, G.G., Fitzpatrick, N., Marras, W.S., 2016. MRI Cross Sectional Atlas of Normal Canine Cervical Musculoskeletal Structure. Submitted for publication.

446 Autefage, A., Palierne, S., Charron, C., Swider, P., 2012. Effective mechanical properties of diaphyseal
447 cortical bone in the canine femur. Vet. J. Lond. Engl. 1997 194, 202–209.
448 doi:10.1016/j.tvjl.2012.04.001
449 Breit, S., Künzel, W., 2004. A Morphometric Investigation on Breed-Specific Features Affecting Sagittal
450 Rotational and Lateral Bending Mobility in the Canine Cervical Spine (C3–C7). Anat. Histol.
451 Embryol. 33, 244–250. doi:10.1111/j.1439-0264.2004.00546.x
452 Choi, H., Vanderby Jr, R., 1999. Comparison of Biomechanical Human Neck Models: Muscle Forces and
453 Spinal Loads at C4/5 Level. J. Appl. Biomech. 15, 120–138. doi:10.1016/S1350-4533(02)00151-0
454 Cholewicki, J., McGill, S.M., 1994. EMG assisted optimization: A hybrid approach for estimating muscle
455 forces in an indeterminate biomechanical model. J. Biomech. 27, 1287–1289. doi:10.1016/0021-
456 9290(94)90282-8
457 Cholewicki, J., McGill, S.M., Norman, R.W., 1995. Comparison of muscle forces and joint load from an
458 optimization and EMG assisted lumbar spine model: towards development of a hybrid approach.
459 J. Biomech. 28, 321–331.
460 Crisco, J.J., Panjabi, M.M., Wang, E., Price, M.A., Pelker, R.R., 1990. The injured canine cervical spine
461 after six months of healing. An in vitro three-dimensional study. Spine 15, 1047–1052.
462 Dufour, J.S., Marras, W.S., Knapik, G.G., 2013. An EMG-assisted model calibration technique that does
463 not require MVCs. J. Electromyogr. Kinesiol. Off. J. Int. Soc. Electrophysiol. Kinesiol. 23, 608–613.
464 doi:10.1016/j.jelekin.2013.01.013
465 Dugailly, P.-M., Sobczak, S., Moiseev, F., Sholukha, V., Salvia, P., Feipel, V., Rooze, M., Van Sint Jan, S.,
466 2011. Musculoskeletal modeling of the suboccipital spine: kinematics analysis, muscle lengths,
467 and muscle moment arms during axial rotation and flexion extension. Spine 36, E413–422.
468 doi:10.1097/BRS.0b013e3181dc844a
469 Dumas, G.A., Poulin, M.J., Roy, B., Gagnon, M., Jovanovic, M., 1991. Orientation and moment arms of
470 some trunk muscles. Spine 16, 293–303.
471 Foss, K., da Costa, R.C., Moore, S., 2013. Three-dimensional kinematic gait analysis of Doberman
472 Pinschers with and without cervical spondylomyelopathy. J. Vet. Intern. Med. Am. Coll. Vet.
473 Intern. Med. 27, 112–119. doi:10.1111/jvim.12012
474 Granata, K.P., Marras, W.S., 1995. An EMG-assisted model of trunk loading during free-dynamic lifting. J.
475 Biomech. 28, 1309–1317.
476 Granata, K.P., Marras, W.S., 1993. An EMG-assisted model of loads on the lumbar spine during
477 asymmetric trunk extensions. J. Biomech. 26, 1429–1438. doi:10.1016/0021-9290(93)90093-T
478 Han, I.S., Kim, Y.E., Jung, S., 2012. Finite element modeling of the human cervical spinal column: Role of
479 the uncovertebral joint. J. Mech. Sci. Technol. 26, 1857–1864. doi:10.1007/s12206-012-0427-2
480 Horst, M.J. van der, Thunnissen, J.G.M., Happee, R., Haaster, R.M.H.P. van, Wismans, J.S.H.M., 1997. The
481 Influence of Muscle Activity on Head-Neck Response During Impact (SAE Technical Paper No.
482 973346). SAE Technical Paper, Warrendale, PA.
483 Huber, Z.E., 2013. Creation and Validation of a Dynamic, EMG-Driven Cervical Spine Model. The Ohio
484 State University.
485 Hyeonki Choi, R.V.J., 2010. Comparison of Biomechanical Human Neck Models: Muscle Forces and Spinal
486 Loads at C4/5 Level [WWW Document]. Hum. Kinet. J. URL
487 http://journals.humankinetics.com/jab-back-issues/jabvolume15issue2may/comparison-of-
488 biomechanical-human-neck-models-muscle-forces-and-spinal-loads-at-c45-level (accessed
489 12.17.15).
490 Jaeger, R., Mauch, F., Markert, B., 2011. The muscle line of action in current models of the human
491 cervical spine: a comparison with in vivo MRI data. Comput. Methods Biomech. Biomed. Engin.
492 15, 953–961. doi:10.1080/10255842.2011.567982

493 Jager, M. de, Sauren, A., Thunnissen, J., Wismans, J., 1996. A Global and a Detailed Mathematical Model
494 for Head-Neck Dynamics. Proceeding Thw 30th Stapp Car Crash Conf. SAE Paper No. 962430,
495 269–281.
496 Jaumard, N.V., Welch, W.C., Winkelstein, B.A., 2011. Spinal facet joint biomechanics and
497 mechanotransduction in normal, injury and degenerative conditions. J. Biomech. Eng. 133,
498 071010. doi:10.1115/1.4004493
499 Jeffery, N. d., Levine, J. m., Olby, N. j., Stein, V. m., 2013. Intervertebral Disk Degeneration in Dogs:
500 Consequences, Diagnosis, Treatment, and Future Directions. J. Vet. Intern. Med. 27, 1318–1333.
501 doi:10.1111/jvim.12183
502 Johnson, J.A., da Costa, R.C., Bhattacharya, S., Goel, V., Allen, M.J., 2011. Kinematic motion patterns of
503 the cranial and caudal canine cervical spine. Vet. Surg. VS 40, 720–727. doi:10.1111/j.1532-
504 950X.2011.00853.x
505 Jorgensen, M.J., Marras, W.S., Gupta, P., 2003. Cross-sectional area of the lumbar back muscles as a
506 function of torso flexion. Clin. Biomech. Bristol Avon 18, 280–286.
507 Kumar, M.S.A., 2012. Clinically Oriented Anatomy of the Dog and Cat. Linus Publications, Ronkonkoma,
508 NY 11779.
509 Lim, T.H., Goel, V.K., Weinstein, J.N., Kong, W., 1994. Stress analysis of a canine spinal motion segment
510 using the finite element technique. J. Biomech. 27, 1259–1269.
511 Lopik, D.W. van, Acar, M., 2007. Development of a multi-body computational model of human head and
512 neck. Proc. Inst. Mech. Eng. Part K J. Multi-Body Dyn. 221. doi:10.1243/14644193JMBD84
513 Macintosh, J.E., Bogduk, N., 1991. The attachments of the lumbar erector spinae. Spine 16, 783–792.
514 Marras, W.S., Davis, K.G., 2001. A non-MVC EMG normalization technique for the trunk musculature:
515 Part 1. Method development. J. Electromyogr. Kinesiol. Off. J. Int. Soc. Electrophysiol. Kinesiol.
516 11, 1–9.
517 Marras, W.S., Granata, K.P., 1997. The development of an EMG-assisted model to assess spine loading
518 during whole-body free-dynamic lifting. J. Electromyogr. Kinesiol. Off. J. Int. Soc. Electrophysiol.
519 Kinesiol. 7, 259–268.
520 McCully, K.K., Faulkner, J.A., 1983. Length-tension relationship of mammalian diaphragm muscles. J.
521 Appl. Physiol. 54, 1681–1686.
522 Németh, G., Ohlsén, H., 1986. Moment arm lengths of trunk muscles to the lumbosacral joint obtained
523 in vivo with computed tomography. Spine 11, 158–160.
524 Sharir, A., Milgram, J., Shahar, R., 2006. Structural and functional anatomy of the neck musculature of
525 the dog (Canis familiaris). J. Anat. 208, 331–351. doi:10.1111/j.1469-7580.2006.00533.x
526 Sheng, S.-R., Wang, X.-Y., Xu, H.-Z., Zhu, G.-Q., Zhou, Y.-F., 2010. Anatomy of large animal spines and its
527 comparison to the human spine: a systematic review. Eur. Spine J. Off. Publ. Eur. Spine Soc. Eur.
528 Spinal Deform. Soc. Eur. Sect. Cerv. Spine Res. Soc. 19, 46–56. doi:10.1007/s00586-009-1192-5
529 Snijders, C.J., Hoek van Dijke, G.A., Roosch, E.R., 1991. A biomechanical model for the analysis of the
530 cervical spine in static postures. J. Biomech. 24, 783–792.
531 Soret, M., Bacharach, S.L., Buvat, I., 2007. Partial-volume effect in PET tumor imaging. J. Nucl. Med. Off.
532 Publ. Soc. Nucl. Med. 48, 932–945. doi:10.2967/jnumed.106.035774
533 Stemper, B.D., Yoganandan, N., Pintar, F.A., 2004. Validation of a head-neck computer model for
534 whiplash simulation. Med. Biol. Eng. Comput. 42, 333–338.
535 Theado, E.W., Knapik, G.G., Marras, W.S., 2007. Modification of an EMG-assisted biomechanical model
536 for pushing and pulling. Int. J. Ind. Ergon., Musculoskeletal Load of Push–Pull Tasks 37, 825–831.
537 doi:10.1016/j.ergon.2007.07.012
538 Vasavada, A.N., Li, S., Delp, S.L., 1998. Influence of muscle morphometry and moment arms on the
539 moment-generating capacity of human neck muscles. Spine 23, 412–422.

Zimmerman, M.C., Vuono-Hawkins, M., Parsons, J.R., Carter, F.M., Gutteling, E., Lee, C.K., Langrana, N.A., 1992. The mechanical properties of the canine lumbar disc and motion segment. Spine 17, 213–220.

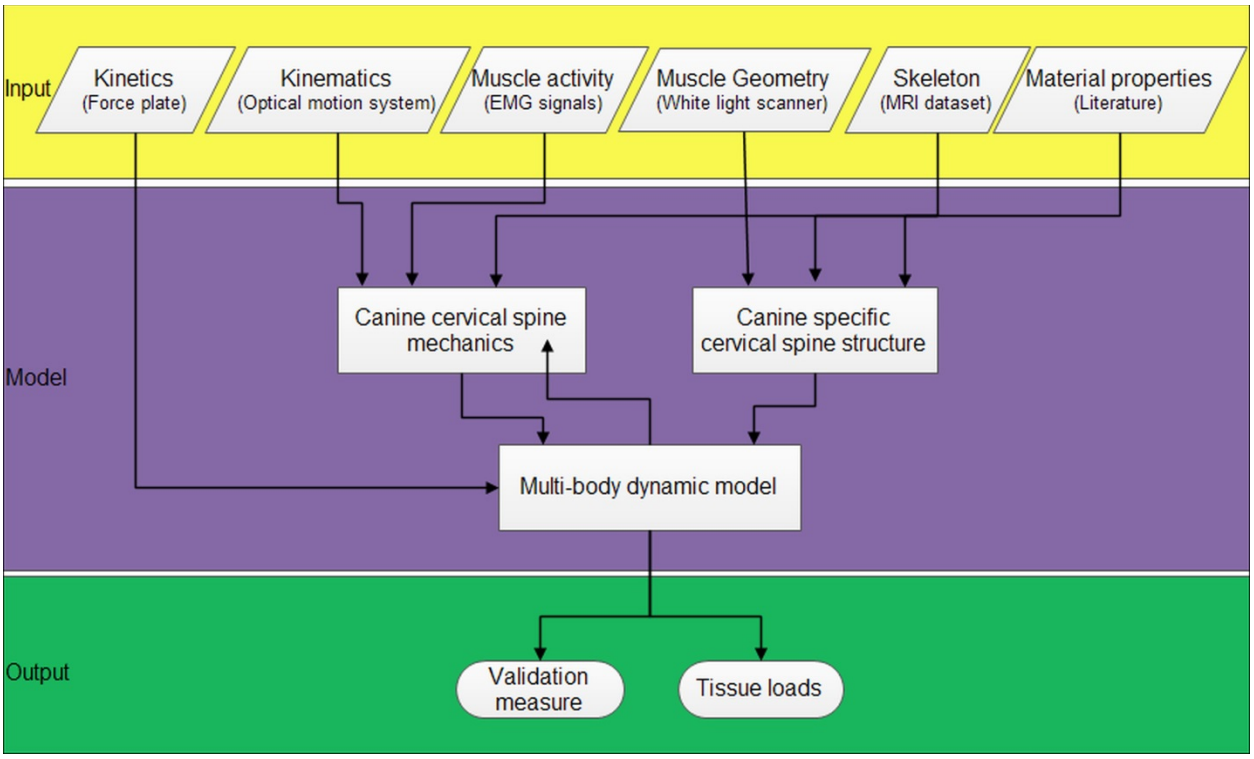

Figure.1 This graphic displays the overall modeling logic.

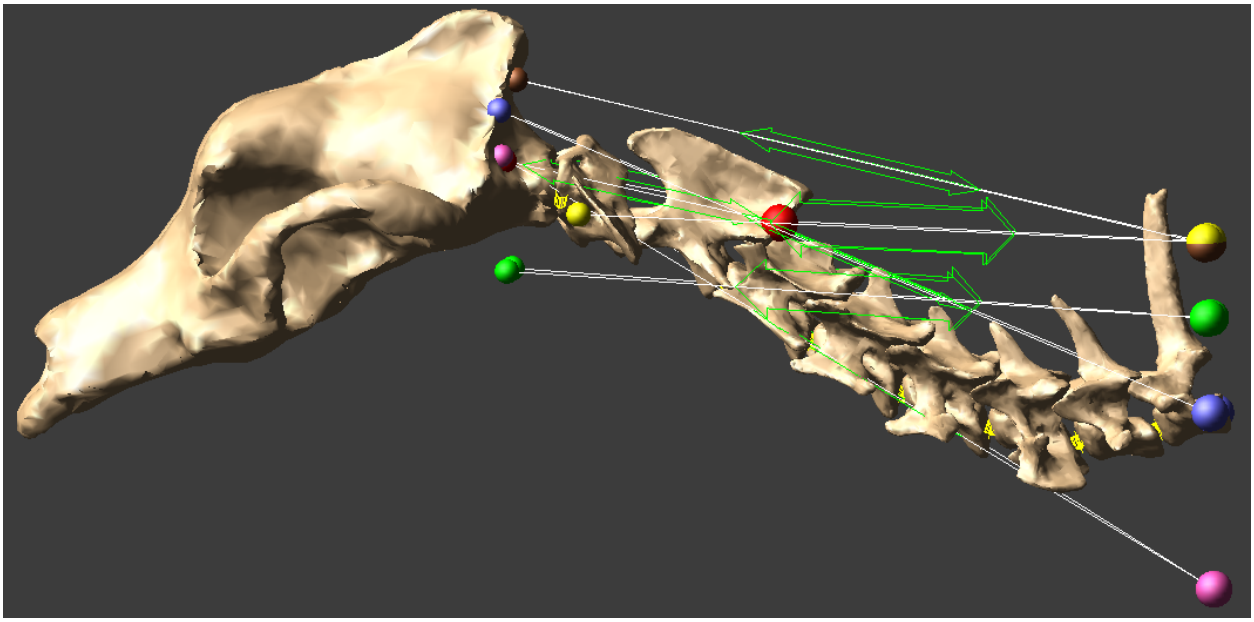

Figure 2. Dynamic model of canine cervical spine with straight line muscles. (a) Side view. (b) Top view. longissimus, complexus, sternocleidomastoid, splenius, obliquus capitis, biventer.

Figure 3. The latex resistance band (TheraBand, Akron, OH, USA) connected to the neck of the subject from one end and to the force plate from the other end. The subject was naturally pulling against the latex resistance band in order to eat the food treat.

584 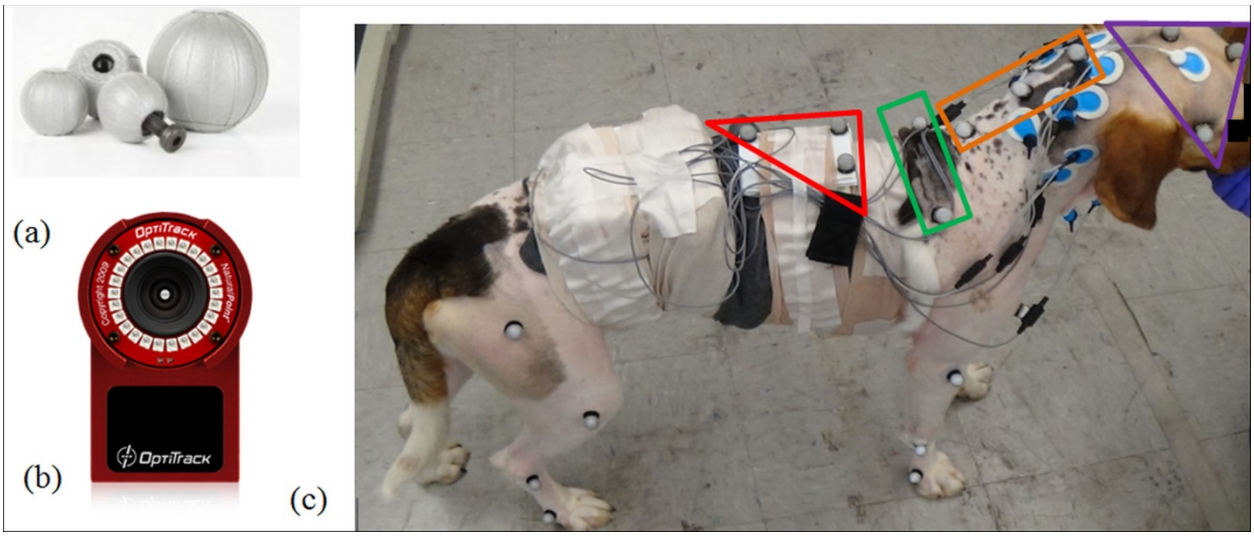

585 **Figure 4.** (a) Optical markers. (b) Optical motion capture camera. (c) Location of optical
586 markers in order to measure joint angles: Head markers, Neck markers, Shoulder markers,
587 UpperTorso markers

588

589

590

591

592

593

594

595

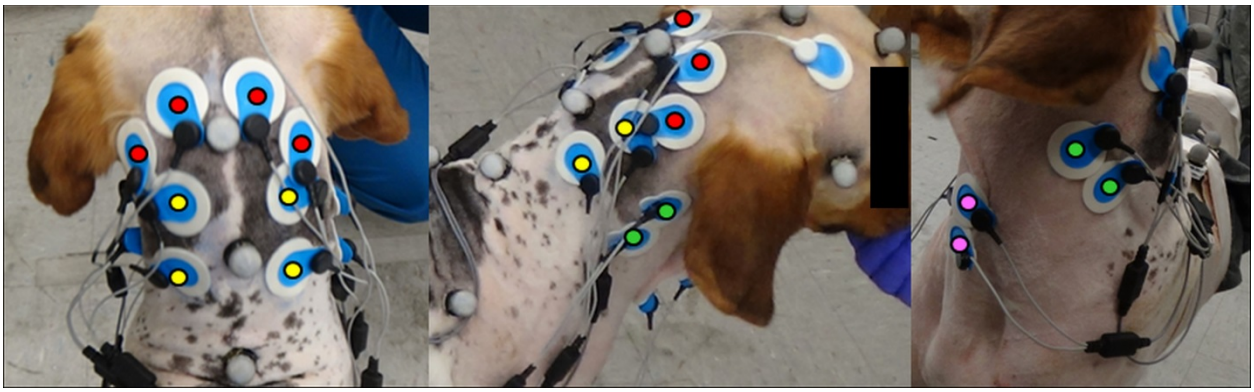

Figure 5. Surface electromyography (EMG) electrode location, Obliquus capitis, Splenius, Longissimus, Sternocleidomastoideus

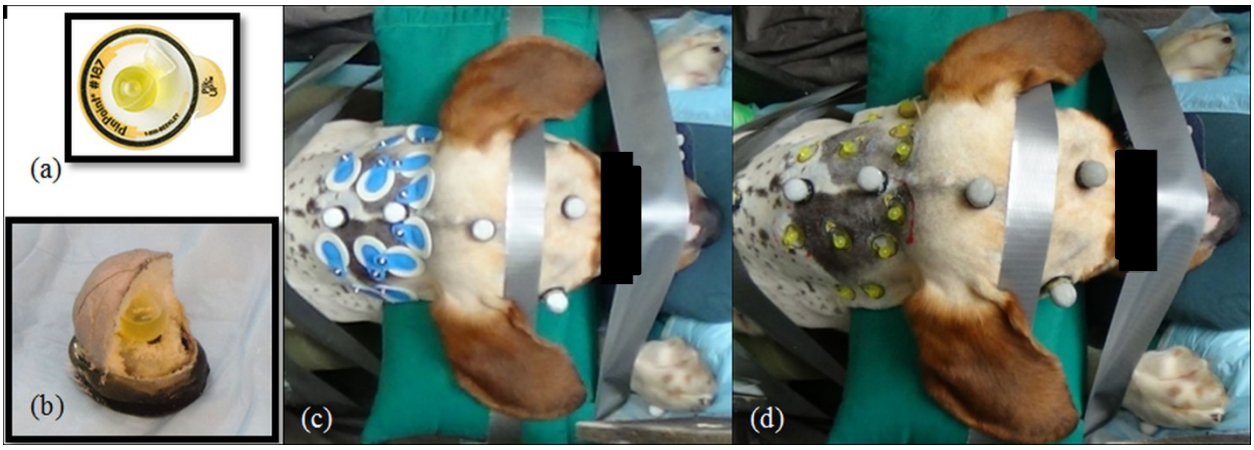

Figure 6. (a) MRI diagnostic marker, (b) Dual modality marker (cut in half for clarity), (c) location of EMG electrodes and dual modality markers, (d) replaced EMG electrodes with MRI diagnostic marker.

(a)

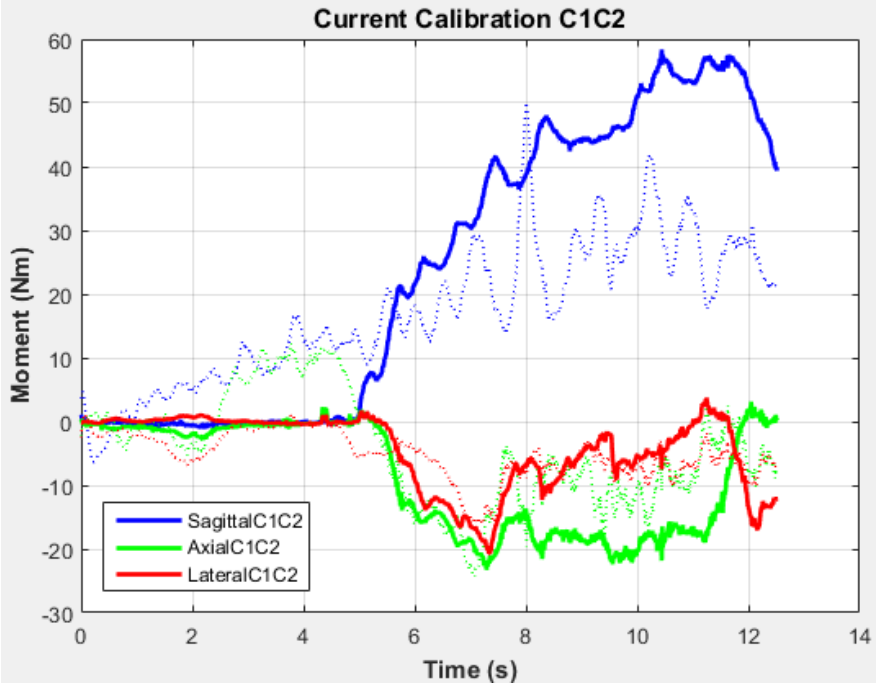

(b)

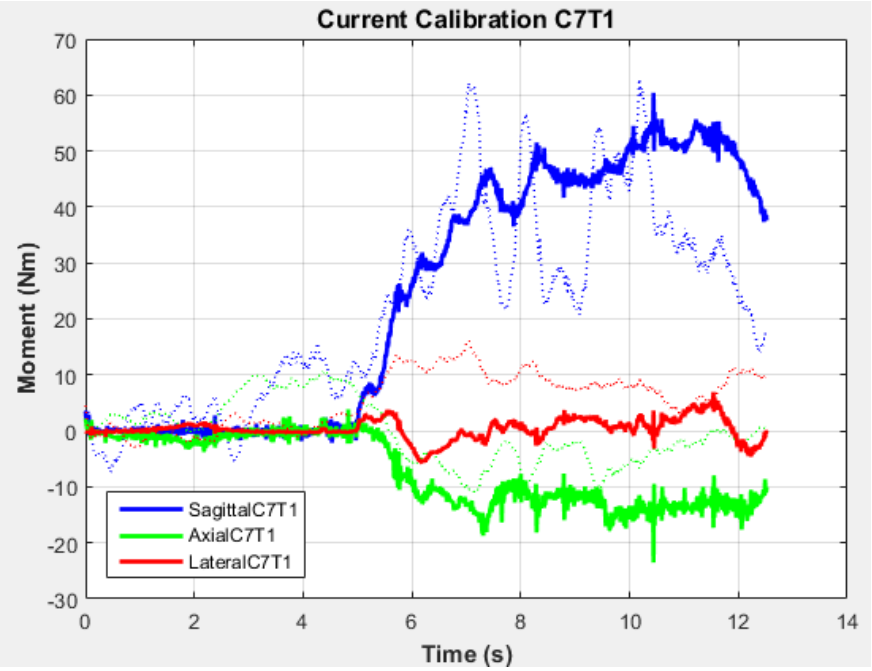

Figure 7. Canine cervical spine measured external moments (solid lines) as a function of time during a typical exertion and the moments predicted from the EMG-assisted model for the calibration trial (dashed lines). (a) C1C2 level. (b) C7T1 level. Blue = Sagittal plane, Green = Axial plane, Red = Lateral plane.

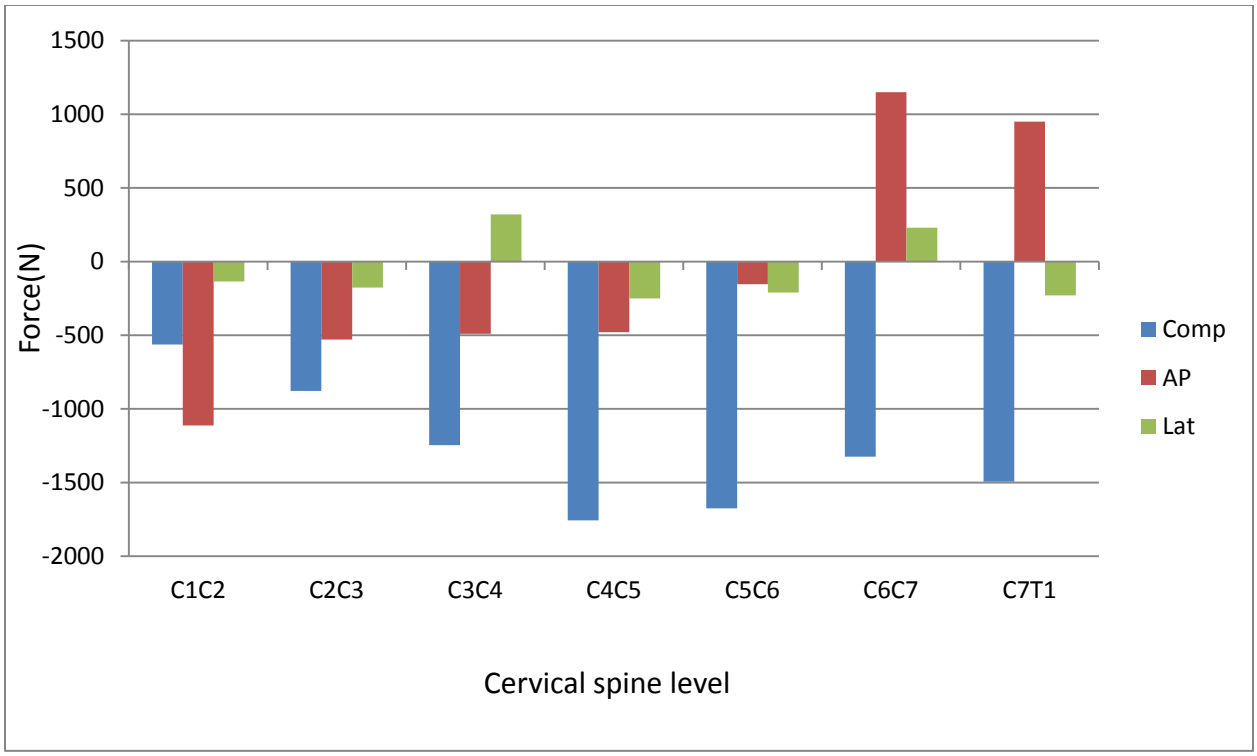

630

631 **Figure 8**. Maximum Spinal load during the trial at each level (comp=Compression,

632 AP=Anterior-posterior shear, Lat= Lateral shear).

633